

## Prestress Monitoring of Internal Steel Strands Using the Magnetoelastic Inductance Method

Lei Liu<sup>1, 2</sup>, Senhua Zhang<sup>1, 2</sup>, Jianting Zhou<sup>1, 2</sup>, Hong Zhang<sup>1, 2</sup>, Huiling Liu<sup>1, 2</sup>,  
Kui Tan<sup>1, 2</sup>, and Leng Liao<sup>1, 3, \*</sup>

**Abstract**—Monitoring the prestress of prestressed steel strands is important but difficult. The magnetoelastic inductance (MI) method is used to monitor the prestress. A coupling model was established to describe the correlation among stress, magnetism, and inductance. A prestress monitoring system based on the MI effect was proposed. To verify the feasibility of the method, experiments were carried out. The results showed that influenced by the hydration heat of the grouting materials, the fluctuation range of the inductance was 1.033%. When the hydration came to an end, the inductance approached the initial inductance. For internal steel strands, the obtained inductance-prestress relationship was similar to the relationship of external steel strands. Thus, the prestress of the internal steel strands could be monitored by the MI method.

### 1. INTRODUCTION

Prestressed concrete structures use prestress to overcome the problem of the low tensile strength of concrete. The prestress effectively improves the bearing capacity and durability. During the construction and service of structures, the prestress of the internal steel strands changes. To ensure the bearing capacity and durability of structures, it is very important to obtain its prestress [1].

For the nondestructive testing and monitoring of the prestress, researchers have proposed a variety of methods, including vibration frequency method, acoustic emission method, ultrasonic method, stress wave method, eddy current method, electromagnetic oscillation method, and magnetoelastic method. The vibration frequency method [2] derives the change of the prestress by the measured vibration frequency of the structure. The prestress determined by the vibration frequency is the prestress of the structure. The prestress of different steel strands or at difficult sections cannot be obtained. Moreover, the factors that cause vibration frequency changes are complicated. Figuring out the influence of the prestress is difficult. The acoustic emission method [3, 4], a passive method, uses emitted elastic waves to determine the prestress. The ultrasonic method is based on the acoustoelastic effect, which points out the relationship between stress and wave velocity. Bartoli et al. [5] used the frequency change of ultrasonic guided waves to detect the prestress. Since the steel strand was not a cylinder, the propagation of guided waves inside the steel strand has not been analyzed. Besides, internal steel strands were wrapped by grouting materials. The propagation of ultrasonic waves was hindered. When long steel strands are tested, the signal-to-noise ratio of the ultrasonic signal is not high. Based on the acoustoelastic effect, Chen et al. [6] used the traveling time of stress waves over the entire length of the strand to characterize the steel stress. Besides, a steel strand with a length of 80 m was tested by the stress wave method.

---

*Received 9 April 2021, Accepted 3 June 2021, Scheduled 9 June 2021*

\* Corresponding author: Leng Liao (lengliao@cqjtu.edu.cn).

<sup>1</sup> State Key Laboratory of Mountain Bridge and Tunnel Engineering, Chongqing Jiaotong University, Chongqing 400074, China.

<sup>2</sup> College of Civil Engineering, Chongqing Jiaotong University, Chongqing 400074, China. <sup>3</sup> College of Materials Science and Engineering, Chongqing Jiaotong University, Chongqing, China.

The magnetoelastic effect [7] describes the relationship between the stress and the magnetization of ferromagnetic materials. Based on the magnetoelastic effect, the magneto-elastic effect method, eddy current method, and electromagnetic oscillation method are proposed. To test the stress of steel bars, Schoenekess et al. [8] proposed an eddy current sensor. Using the eddy current method, Kim et al. [9] realized the automatic measurement of the prestress of steel strands. Affected by the skin effect, the test depth of the eddy current method is limited. The electromagnetic oscillation method [10] takes the steel strand as an inductor, which was connected to the test circuit to form an LC circuit. The resonance frequency of the LC circuit was used as an indicator of the prestress. Because the inductance of the steel strand was small, the stress-caused change in the inductance and the resonance frequency were small. Thus, the sensitivity of this method was low, resulting in a high requirement for the monitoring environment.

The magnetoelastic method [11,12] measures the magnetic flux to calculate the stress of steel strands. To provide a strong excitation magnetic field to magnetize the steel strand to a saturated state [13], traditional magnetoelastic sensors have a large size and high requirements for the power supply. Therefore, the magnetoelastic sensors, proposed by Wang [11] and Duan et al. [14], were used for cable tension monitoring. To reduce the size of the magnetoelastic sensor, the magnetoelastic inductance method [15] (MIM) was proposed. In previous studies, the relationship between stress and inductance was analyzed. However, the theoretical analysis was carried out combining the Joule effect and the definition of the inductance. Due to the small size of the MIM sensor, the MIM method could be used for prestress monitoring. Experimental research was conducted on external steel strands [16]. Because the internal steel strands are wrapped by grouting material, the working condition of the MIM sensor is different. To monitor the prestress of internal steel strands by the MIM method, the influence of the grouting material and the working environment must be clarified.

In this paper, the correlation among stress, magnetization, and inductance was analyzed. A stress-magnetization-inductance coupling model was established to describe the correlation. Based on this, the prestress monitoring system based on the MIM was proposed. To verify the feasibility of the MIM method for prestress monitoring, prestress monitoring experiments were carried out. The prestress of the steel strands within the grouting material and the prestressed concrete beam were monitored. The experimental results demonstrated that the MIM sensor was influenced by the hydration heat of the grouting material. When the hydration came to an end, the influence of the grouting material diminished, and the inductance of the MIM sensor was restored. For the sensor embedded within the prestress duct, the inductance-prestress relationship was similar to that of the sensor in the air. Thus, the prestress calculation method proposed for external steel strands could be used for internal steel strands. The applicability of the MIM to prestress monitoring on internal steel strands was verified. The application of the MIM method was expanded, and a new method for prestress monitoring was provided.

## 2. THEORY BACKGROUND

### 2.1. Coupling of Stress and Magnetization

According to the magnetoelastic effect, the magnetization ( $M$ ) of steel strand is related to the excitation magnetic field ( $H$ ), stress ( $\sigma$ ), and temperature ( $T$ ) [17]. When the excitation magnetic field and temperature remain unchanged, the magnetization can be expressed as Eq. (1).

$$\frac{dM}{dt} = \frac{\partial M}{\partial \sigma} \frac{\partial \sigma}{\partial t} \quad (1)$$

The J-A model [18] points out that the stress-induced magnetization includes reversible magnetization ( $M_{re}$ ) and irreversible magnetization ( $M_{inre}$ ). The reversible magnetization and irreversible magnetization are given by Eq. (2) and Eq. (3), respectively [18]. In the equations,  $\delta$  represents the change of the excitation magnetic field,  $k$  the pinning coefficient,  $\alpha$  the demagnetization coefficient, and  $c$  the reversible magnetic susceptibility. The magnetization without hysteresis,  $M_a$ , is expressed as Eq. (4), where  $a$  characterizes the degree of inclination of the hysteresis curve;  $M_s$  is the

saturation magnetization;  $H_e$  is the effective magnetic field.

$$\frac{dM_{inre}}{dH} = \frac{M_a - M_{inre}}{k\delta - \alpha(M_a - M_{inre})} \quad (2)$$

$$M_{re} = c(M_a - M_{inre}) \quad (3)$$

$$M_a(H) = M_s \left( \coth \left( \frac{H_e}{a} - \frac{a}{H_e} \right) \right) \quad (4)$$

Since the excitation magnetic field and temperature remain unchanged, the effective magnetic field is determined by the stress-induced magnetic field ( $H_\sigma$ ) [19]:

$$H_e = H + \alpha M + \frac{3\sigma}{2\mu_0} \frac{d\lambda}{dM} + \frac{S}{\mu_0} \frac{dT}{dM} = H + \alpha M + H_\sigma + H_T \quad (5)$$

In Eq. (5),  $H_T$  is the temperature-induced magnetic field. Because the magnetic domain structure of steel strands is complex, the magnetostriction coefficient ( $\lambda$ ) is difficult to describe analytically. Thus, an empirical equation [20], Eq. (6), is used to calculate the magnetostriction coefficient. Combining Eq. (5) and Eq. (6), the stress-induced magnetic field can be expressed as Eq. (7).

$$\lambda = \Sigma \left[ \gamma_i(0) \sum_{n=1}^{\infty} \frac{\sigma^n}{n!} \gamma_i^{(n)}(0) \right] M^{2i} \quad (6)$$

$$H_\sigma = \frac{3\sigma}{\mu_0} \sum_{i=0}^{\infty} i \left( M^{2i-1} \sum_{n=0}^{\infty} \frac{\sigma^n}{n!} \gamma_i^{(n)}(0) \right) \quad (7)$$

According to Eq. (3), before determining the reversible magnetization, the irreversible magnetization should be determined. The coupling of stress and magnetization is essentially the energy conversion [19]. The conversion between the irreversible magnetization and elastic energy satisfies Eq. (8), where  $\nu$  is a parameter related to the energy per unit volume, and  $W$  is the deformation energy per unit volume. Combining Eqs. (2), (3), and (8), the change rate of the magnetization to unit volume deformation is given by Eq. (9).

$$\nu \frac{dM_{inre}}{dW} = (M_a - M_{inre}) \quad (8)$$

$$\frac{dM}{dW} = \frac{d(c(M_a - M_{inre}) + M_{inre})}{dW} = c \frac{dM_a}{dW} + \frac{(1-c)}{\nu} (M_a - M_{inre}) \quad (9)$$

Taken the tensed steel strand as isotropic, when the stress is less than its non-proportional extension strength, the deformation energy per unit volume is expressed as Eq. (10). Combining Eq. (9) and Eq. (10), the relationship between magnetization and stress is defined by Eq. (11).

$$W = \frac{\sigma^2}{2E} \quad (10)$$

$$\frac{dM}{d\sigma} = \frac{\sigma}{\nu E} (M_a - M) + c \frac{dM_a}{d\sigma} \quad (11)$$

When the magnetization of the steel strand is obtained, the magnetic permeability ( $\mu$ ) of the steel strand is calculated as:

$$\mu = \mu_0 \frac{(H + M)}{H} \quad (12)$$

## 2.2. Coupling of Magnetization and Inductance

According to the Biot-Savart theory, the coil of the magnetoelastic inductance sensor [16] can be regarded as a solenoid. The solenoid has a radius of  $r$ , a length of  $l_m$ , and turns of  $n$ . Assuming that the magnetic field distributes uniformly along the coil's axis, the magnetic field in the coil ( $B$ ) can be expressed as

Eq. (13). When there is no iron core inside the sensor, the inductance of the coil,  $L_{coil}$ , is given by Eq. (14).

$$B = \frac{\mu_0 n I}{2l_m^2} \left( (r^2 + l_m^2)^{1/2} - r \right) \quad (13)$$

$$L_{coil} = \frac{n B \pi r^2}{I} = \frac{\mu_0 n^2 \pi r^2}{2l_m^2} \left( (r^2 + l_m^2)^{1/2} - r \right) \quad (14)$$

The steel strand could be simplified as a cylinder with a length of  $l_{iron}$ , a radius of  $r_{iron}$ , and a magnetic permeability of  $\mu$ . When the steel strand is placed inside the sensor, the inductance of the sensor,  $L_{sensor}$ , is determined by Eq. (15).

$$L_{sensor} = \frac{\mu_0 n^2 \pi}{2l_m^2} \left( \mu r_{iron}^2 \left( (r_{iron}^2 + l_{iron}^2)^{1/2} - r_{iron} \right) + r^2 \left( (r^2 + l_m^2)^{1/2} - r \right) \right) \quad (15)$$

### 2.3. Stress-Magnetization-Inductance Coupling Model

Combine Eqs. (4), (5), (7), (11), (12), and (16), the stress-magnetization-inductance coupling model is obtained. The coupling model can be described by the equation set shown in Eq. (16).

$$\left. \begin{array}{l} \text{Stress-magnetization} \\ \left\{ \begin{array}{l} H_\sigma = \frac{3\sigma}{\mu_0} \sum_{i=0}^{\infty} i \left( M^{2i-1} \sum_{n=0}^{\infty} \gamma_i^{(n)}(0) \right) \\ H_e = H + \alpha M + H_\sigma \\ M_a(H) = M_s \left( \coth \left( \frac{H_e}{a} \right) - \frac{a}{H_e} \right) \\ \frac{dM}{d\sigma} = \frac{\sigma}{vE} (M_a - M) + c \frac{dM_a}{d\sigma} \\ \mu = \mu_0 \frac{H + M}{H} \end{array} \right\} \\ \text{Magnetization-inductance} \quad L_{sensor} = \frac{\mu_0 n^2 \pi}{2l_m^2} \left( \mu r_{iron}^2 \left( (r_{iron}^2 + l_{iron}^2)^{1/2} - r_{iron} \right) \right. \\ \left. + r^2 \left( (r^2 + l_m^2)^{1/2} - r \right) \right) \end{array} \right\} \quad (16)$$

Analytically solving the stress-magnetization-inductance coupling model is difficult. Thus, the coupling model was solved numerically. In the solving process, the excitation current and stress were predetermined. Other parameters were determined according to the properties of the steel strand and the sensor. The aim of solving the coupling model was to verify the relationship between the inductance and stress. Thus, the specific value of the inductance was not important. The parameters, difficult to test, were determined empirically. After the parameters were determined, the coupling model was solved following the steps shown in Fig. 1. The obtained stress-inductance curve was shown in Fig. 2. There was an approximately linear relationship between the inductance and stress. It meant that the sensor inductance can be used to characterize the prestress of the steel strand.

Starting from the basic theories of ferromagnetism and electromagnetics, the basic principles of MIM were analyzed. The stress-magnetization-inductance coupling model was established and solved. This coupling model provided a theoretical basis for the prestress monitoring method based on the magnetoelastic inductance effect.

## 3. EXPERIMENTAL DESIGN

### 3.1. Prestress Monitoring System Using the MIM

To carry out the prestress monitoring experiments, a monitoring system, shown in Fig. 3, was built. The monitoring system consisted of a steel strand, a magnetoelastic inductance sensor, an LCR digital

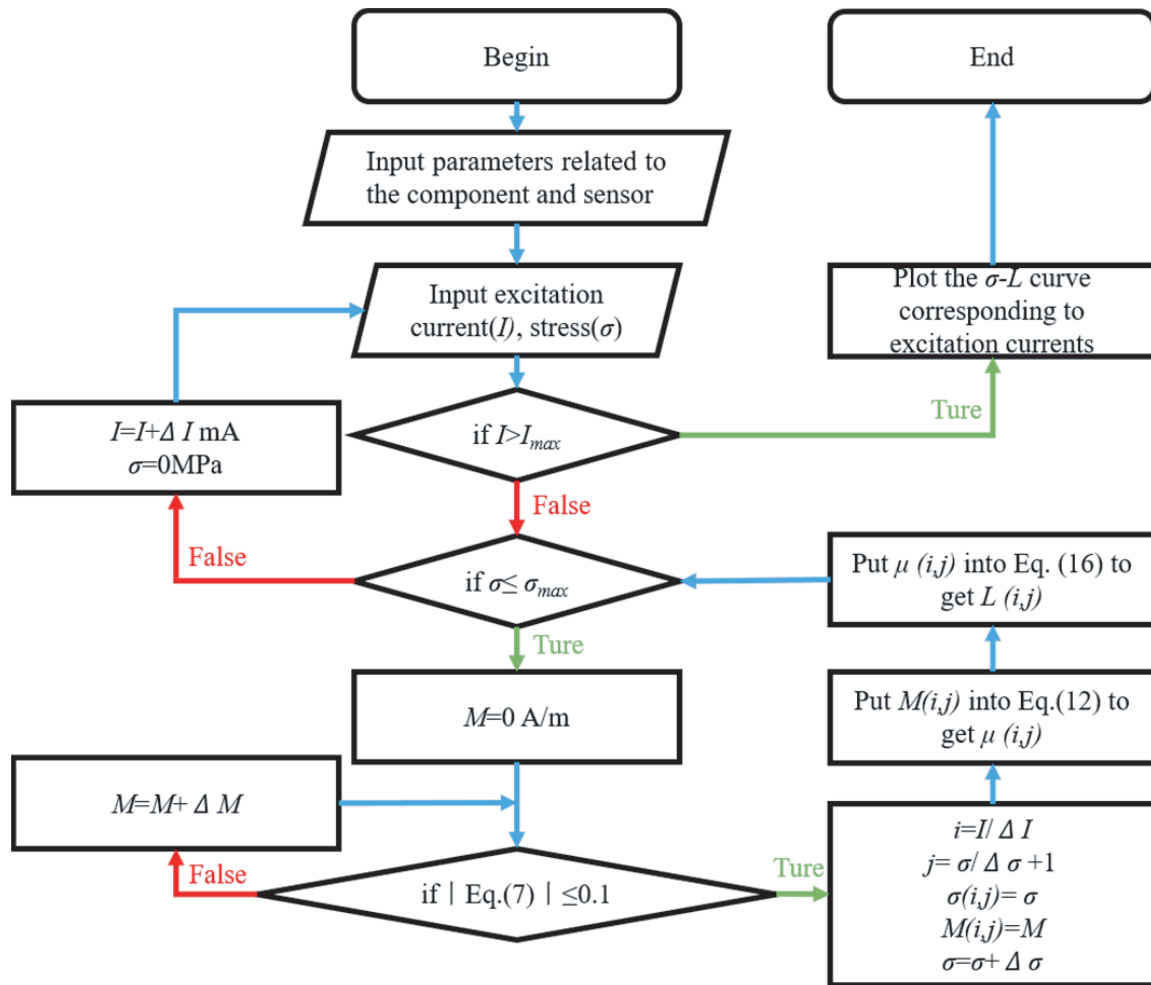


Figure 1. Flow chart of solving the stress-magnetization-inductance coupling model.

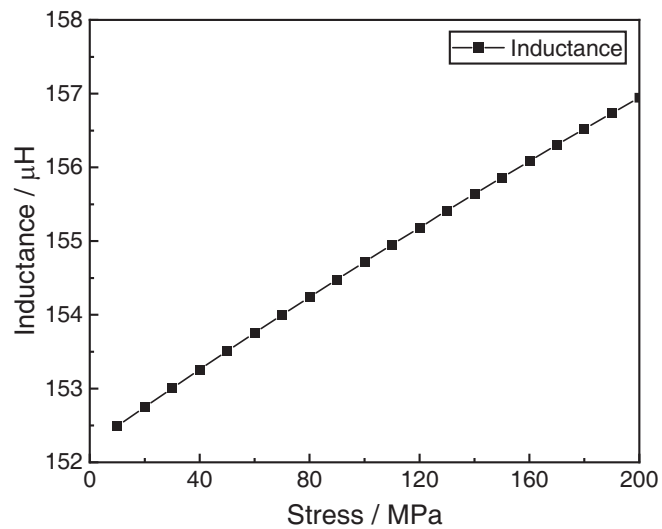
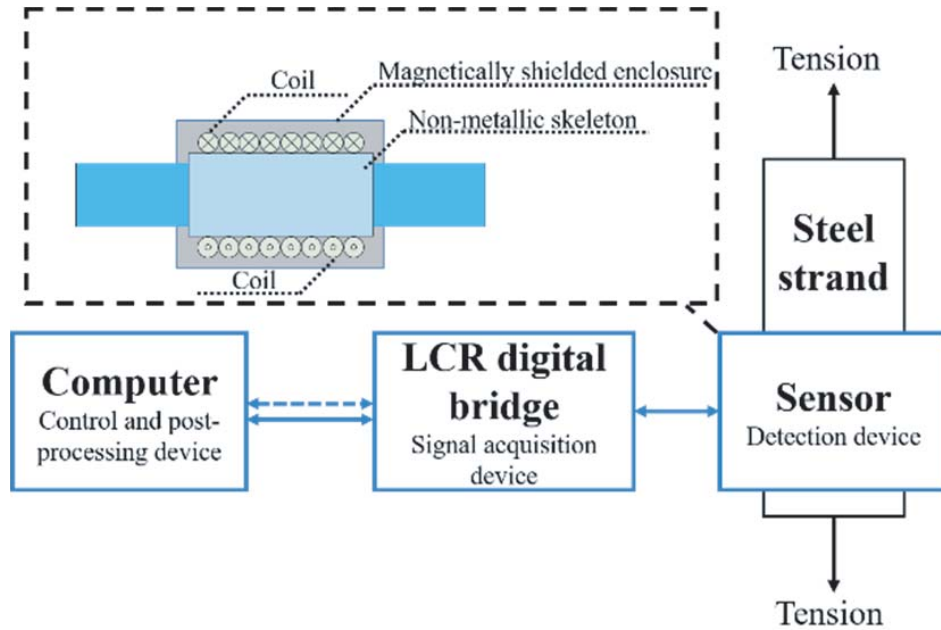


Figure 2. Inductance-stress curve obtained by solving the coupling model.



**Figure 3.** Prestress monitoring system of the MIM.

bridge, and a computer. The magnetoelastic inductance sensor consisted of a coil skeleton, an inductive coil, and a magnetically shielded enclosure. The skeleton was made of non-metallic materials. Regarding the steel strand inside the sensor as an iron core, the sensor and steel strand formed an inductor with an iron core. To test the inductance of the sensor, the sensor was connected to the LCR digital bridge. The measured sensor inductance was transmitted to the computer.

### 3.2. Prestress Monitoring within Prestress Ducts

To figure out the influence of grouting on the prestress monitoring, the experiment was carried out on the steel strands within the prestress duct. In the experiments, the sensors were the same. As shown in Fig. 4, the coil skeleton was a polyvinyl chloride (PVC) pipe with a diameter of 24 mm. Enameled wires with a diameter of 0.35 mm were used to make the coil. The number of coil turns was 200, and the number of winding layers was 1. In the experiments, the sensor enclosure was made by a PVC pipe with a diameter of 32 mm. To prevent the grouting material from flowing into the sensor, the gap at both ends of the sensor was sealed with epoxy resin.

The grouting material was configured with Portland cement and polycarboxylic acid water reducing agent. In the grouting material, the mass ratio of water, cement, and water-reducing agent was 0.3 : 1 : 0.005. Six specimens, whose length was 2 m, were prepared. Since the actual prestressed steel strands have different design tensions, the design tensions of the specimens were different. According to the design tension, the specimens were divided into three groups. As shown in Table 1, each group contained two specimens.

**Table 1.** Label of the specimens.

Label	Design tension / kN	Length / m
A-1/2	0	2
B-1/2	150	2
C-1/2	180	2

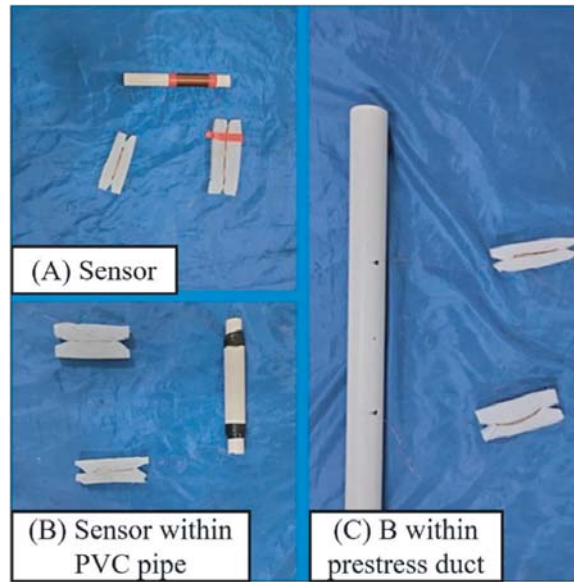


**Figure 4.** Magnetoelastic inductance sensor and the prestressed duct.

The specimens were tensed by a hydraulic jack on a reaction frame. The step of tension was 10 kN. When the steel strand was tensed to different tension levels, the tension was remained to collect the sensor inductance. After the collection was completed, the steel strand was tensed again, until the design tension was reached. As shown in Fig. 5, when the tensioning was completed, a small grouting machine was employed to inject the grout from the grouting hole. When the grout overflow from the vent, the grout injection was completed. The sensor inductance was measured at 0 h, 0.5 h, 1 h, 4 h, 12 h, 24 h after the grout injection. In the next 7 days, the sensor inductance was tested every 12 hours.

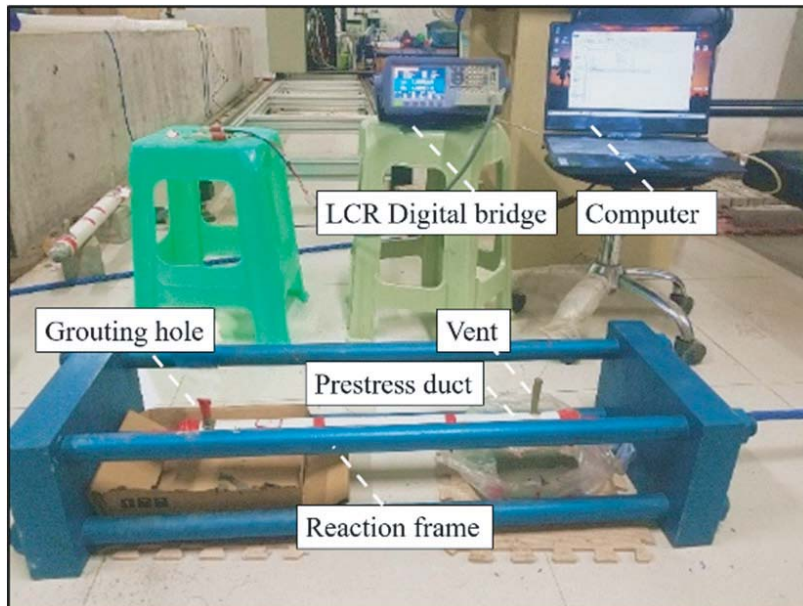


**Figure 5.** Strand tensioning and grout injection.

### 3.3. Prestress Monitoring within a Prestressed Concrete Beam

To verify whether the MIM could be used for the prestress monitoring of actual structures, an experiment was carried out on the steel strands inside a prestressed concrete rectangular beam. As shown in Fig. 6, the prestressed concrete beam was 2000 mm in length, 150 mm in width, and 250 mm in height. The concrete strength was 40 MPa. The longitudinal tensile steel bars had a diameter of 20 mm and a yield strength of 400 MPa. The longitudinal compression steel bars had a diameter of 14 mm and a yield strength of 400 MPa. The diameter of the stirrup was 8 mm, and the spacing between the stirrups was 90 mm. The thickness of the concrete cover was 30 mm. To monitor the prestress at different positions, a magnetoelastic inductance sensor was embedded at the mid-span, and another at the quarter span. To connect the sensors to the LCR digital bridge, two holes were reserved at the sensor positions.

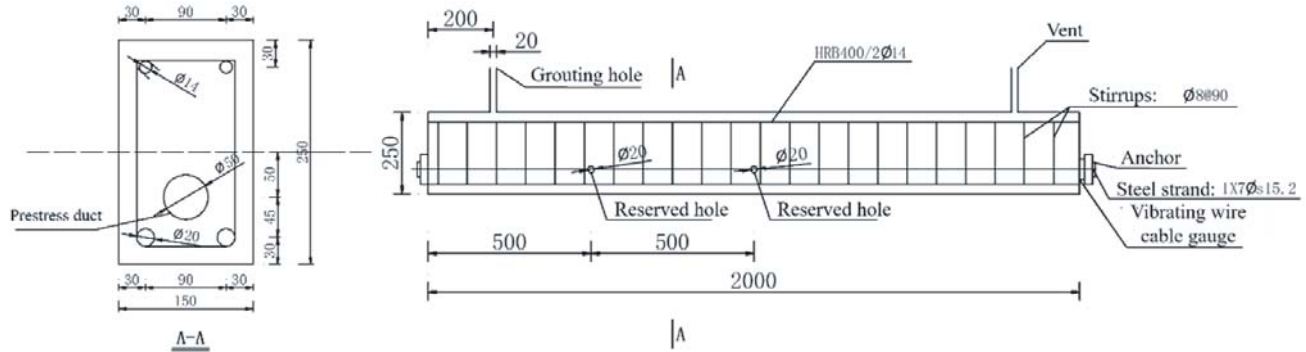


**Figure 6.** Dimensions and reinforcement arrangement of the prestressed concrete beam (Unit: mm).

The concrete beam without prestress was placed on the support. After the steel strand penetrated the prestress duct, the magnetoelastic inductance sensors were fixed at 1/4 span and 1/2 span, respectively. The sensors were connected to the LCR digital bridge through reserved holes. After that, the steel strand was tensed with a step of 10 kN by a hydraulic jack. At each tension level, the tension was maintained to collect the sensor inductance. When the tension reached the design

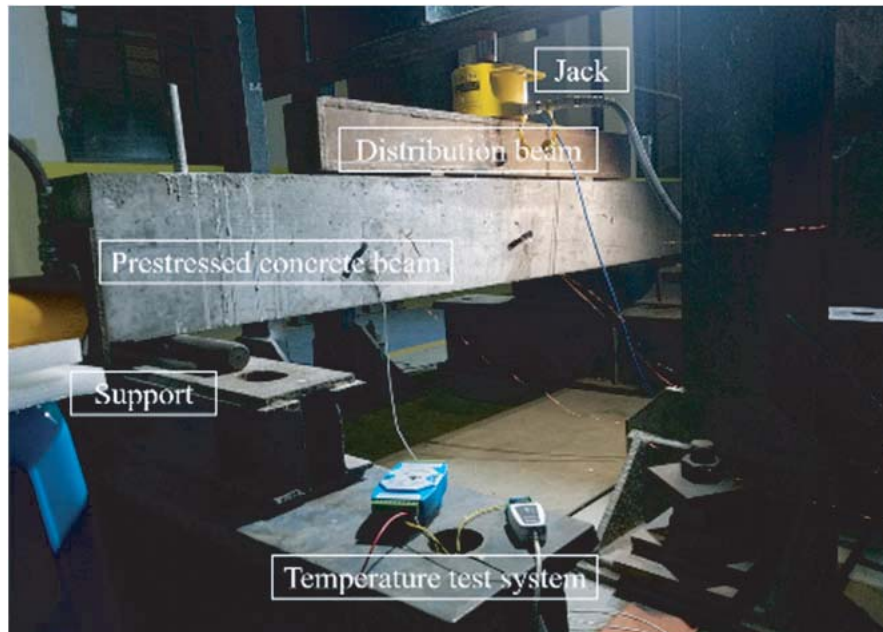


**Figure 7.** Loading by the 4-point bending method.

tension (150 kN), the steel strand was anchored. Then, the grouting material, the same as that used in Section 3.2, was injected from the reserved grouting hole. After the grouting, the sensor inductance was measured. The measuring time was the same as the setting in Section 3.2. As shown in Fig. 7, after 7 days of the grouting, the beam was loaded by the 4-point bending method. The loading aimed to change the prestress of the steel strand, not to destroy the beam. Thus, the maximum load was 200 kN, and the loading step was 10 kN. During the loading process, the sensor inductance was measured at each load level.

## 4. RESULTS AND DISCUSSION

### 4.1. Influence of the Grouting on the Prestress Monitoring

After the grouting, the change in the sensor inductance of each specimen was similar. Thus, specimens A-1 and B-1 were taken for detailed analyses. As shown in Fig. 8, the sensor inductances of A-1 and B-1 differed by about 0.3 mH. This difference was caused by the different tensions of specimens. After the grouting, the sensor inductances of A-1 and B-1 fluctuated. Since A-1 was not tensed, this fluctuation was not caused by the tension change of the steel strand but by its temperature change.

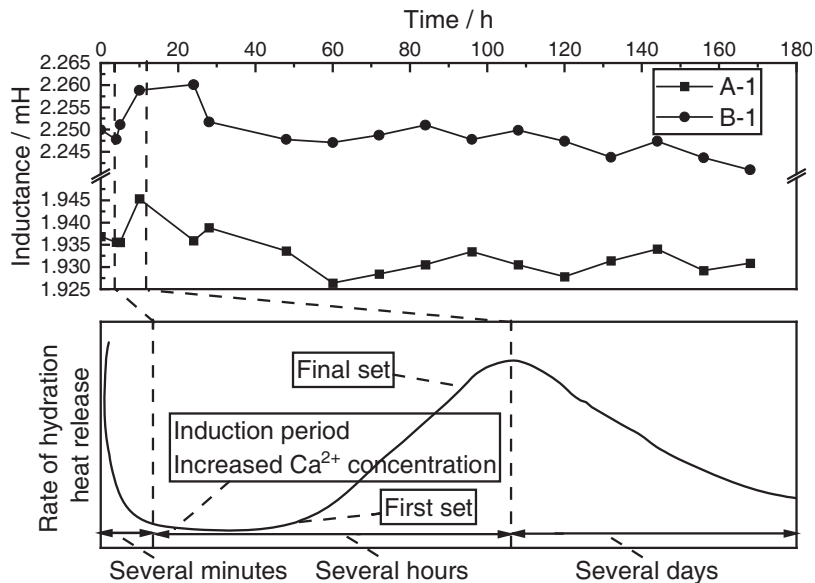


**Figure 8.** Sensor inductance and the rate of hydration heat release.

Because the grouting material contained cement, the hydration reaction of the cement released heat which caused the temperature change of the steel strands. According to the relationship between the heat release rate and the time, the hydration reaction of Portland cement could be divided into three stages. As shown in Fig. 8, with the increase of the hydration reaction time, the sensor inductance and heat release rate changed similarly. In stage 2, a large amount of hydration heat was released, increasing the temperature of the steel strand. According to Eq. (1), the magnetization of steel strands is related to their temperature. Thus, the sensor inductance increased. In stage 3, the heat release rate decreased rapidly. The temperature of the steel strand returned to room temperature. The sensor inductance was gradually restored to the inductance before grouting.

The experimental results demonstrated that the grouting material influenced the sensor inductance. As the hydration heat release rate decreased, the temperature in the prestress duct returned to room temperature. Thus, the sensor inductance was also restored to the inductance before the grouting. For actual structures, the volume and hydration heat of the grouting material were much more than the specimens. Although the influence of the grouting on the sensor inductance would be larger, the influence would last for a few days. When the hydration reaction came to an end, the monitoring results

of the MIM would not be influenced. Thus, magnetoelastic inductance sensors could be embedded into the structure during the construction, and the performance of the sensors could be ensured.

#### 4.2. Prestress Monitoring of Prestressed Concrete Beams

After installing the magnetoelastic inductance sensors in the beam, the steel strand was tensed. As shown in Fig. 9, the inductance increments of the sensors at the 1/2-span and 1/4-span both increased with the increase of the tension. The tension-inductance increment curves corresponding to the sensors differed little. During the loading, the difference in the inductance increments ( $\Delta L$ ) was no more than 3%. This proved that the MIM had good stability, repeatability, and accuracy.

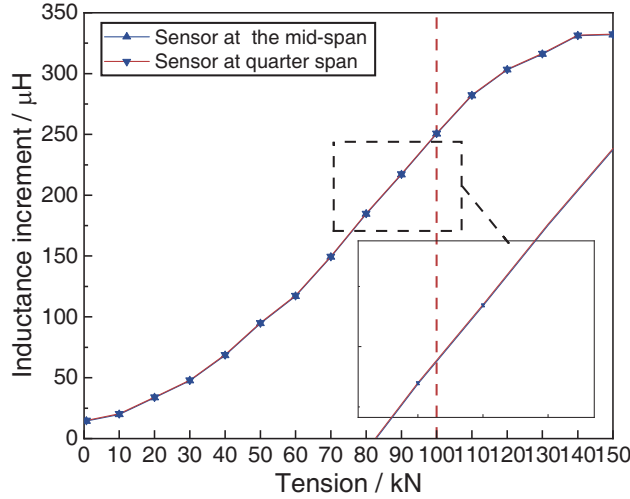


**Figure 9.** Inductance increments of different sensors.

The tension-inductance increment curves could be divided into two stages. In stage 1, the tension increased from 0 kN to 100 kN. In this stage, with the increase in tension,  $\Delta L$  and its changing rate increased. When the tension was 70 kN, the changing rate of  $\Delta L$  reached the maximum. In stage 2,  $\Delta L$  still increased with the tension increment, but the changing rate of the  $\Delta L$  began to decrease. This decrease was caused by the reduction of the sectional area of the steel strand [16]. Since there existed a relationship between  $\Delta L$  and the tension, the sensor inductance could be used to characterize the prestress.

Because the inductance increments of the two sensors differed little, the inductance of the sensor at the mid-span was taken for further analyses. After being tensed to the design tension, the grouting material was injected. In the grouting stage, the sensor inductance fluctuated as shown in Fig. 10. Compared with Fig. 8, it was clear that the change of the sensor inductance coincided with the change of the rate of the hydration heat release. Influenced by the hydration heat, the sensor inductance fluctuated in a small range. With the recovery of the temperature of the steel strand, the sensor inductance approached the inductance which was measured before grouting.

When the temperature of the steel strand returned to room temperature, the beam was loaded. With the load increased, the indication of the cable gauge, installed at the end of the beam, first decreased and then increased. This meant that the prestress of the steel strand was also first decreased and then increased. This was because of the deformation of the beam. With the deformation of the beam, the shape of the steel strand changed. When the load exceeded 60 kN, the prestress of the steel strand increased. As shown in Fig. 11, influenced by the variation of the prestress,  $\Delta L$  reduced from 340.10  $\mu\text{H}$  to 319.29  $\mu\text{H}$ , and then increased to 345.17  $\mu\text{H}$ . During the loading, the relationship between  $\Delta L$  and the prestress was consistent with the  $\Delta L$ -tension curve shown in Fig. 9.

The experimental results showed that for the electromagnetic inductance sensor within the grouting material, its inductance-prestress relationship was similar to that of the sensors exposed in the air. Thus,

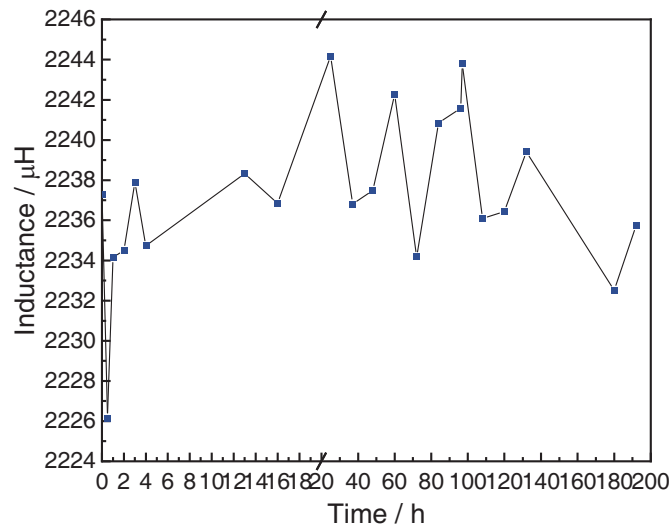


Figure 10. After grouting, the inductance of the sensor at the mid-span.

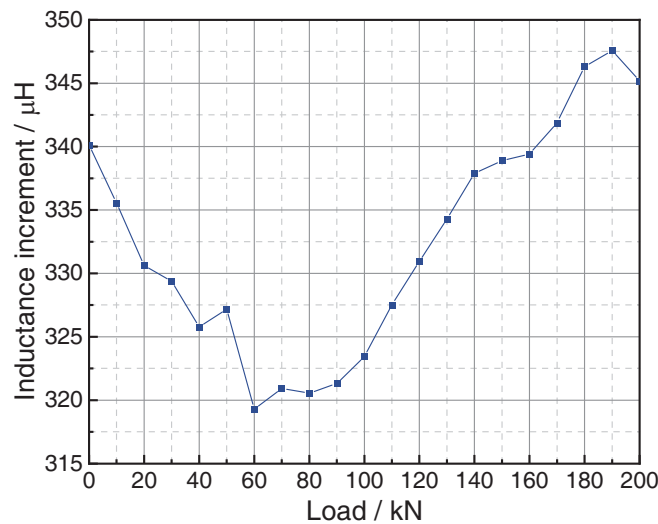


Figure 11. Under loads, the inductance of the sensor at the mid-span.

the MIM could be used to monitor the prestress of the internal steel strand. Additionally, the prestress calculation and analysis method [16, 21] proposed for the external steel strand could be directly used. Because the measured inductance can be affected by uncertainties, a fuzzy preprocessing would be necessary to perform [22, 23].

### 5. CONCLUSIONS AND FUTURE WORK

To monitor the prestress of the internal steel strand by the MIM, the correlation among the stress, magnetization, and inductance was deeply analyzed. A stress-magnetization-inductance coupling model was established to describe the correlation. By numerically solving the coupling model, the nonlinear relationship between the prestress and the sensor inductance was verified. Based on the theoretical analyses, a prestress monitoring system using the MIM was proposed. Prestressed monitoring experiments were carried out to verify the feasibility of the monitoring system.

The experimental results showed that the magnetoelastic inductance sensor embedded in the

structure was influenced by the hydration heat of the grouting material. During the hydration reaction, the sensor inductance fluctuated in a small range. The variation of the sensor inductance was consistent with the rate of the hydration heat release of grouting material. When the hydration reaction came to an end, the sensor inductance returned to the initial value. The influence of grouting material on magnetoelastic inductance sensors could be ignored. Thus, the sensor could be embedded in the structure during the construction, and the performance of the sensor could be ensured.

Under loads, the prestress of the prestressed concrete structures changed. However, there still existed a stable relationship between sensor inductance and the prestress. The obtained inductance-tension curve of the internal sensors was similar to that of the external sensors. Thus, the MIM was suitable for monitoring the prestress of the internal steel strand. The prestress calculation and analysis method proposed for the external steel strand could be directly used.

In this paper, the applicability of the MIM to prestress monitoring on internal steel strands was verified. The application of the MIM method was expanded, and a new method for prestress monitoring was provided. In addition to prestressed steel strands, there are prestressed steel bars in the concrete structure. Because the steel bar was also ferromagnetic, its stress could be monitored by MIM. As the steel bar and steel strand have different stress-strain relationships, it is necessary to revise the existing conclusions of MIM.

## ACKNOWLEDGMENT

This work was supported by the National Natural Science Foundation of China (U20A20314), the Natural Science Fund for Distinguished Young Scholars of Chongqing (cstc2020jcyj-jqX0006), the Chongqing Natural Science Foundation of China (cstc2019jcyj-cxttX0004, cstc2019jscx-gksbX0047, cstc2020yszx-jscxX0003), and the Innovation Fund Project of Graduate Education of Chongqing Jiaotong University (2020S0014).

## REFERENCES

1. Shu, Y., W. Chen, and P. Zhang, et al., "Embedding technology of Fiber Bragg Grating strain sensor for cable tension monitor," *Proceedings of SPIE*, 90440H, 2013.
2. Ho, D., J. Kim, N. Stubbs, et al., "Prestress-force estimation in PSC girder using modal parameters and system identification," *Adv. Struct. Eng.*, Vol. 15, 997–1012, 2016.
3. ElBatanouny, M. K., P. H. Ziehl, A. Larosche, et al., "Acoustic emission monitoring for assessment of prestressed concrete beams," *Constr. Build. Mater.*, Vol. 58, 46–53, 2014.
4. Salamone, S., I. Bartoli, R. Phillips, et al., "Health Monitoring Of Prestressing Tendons In Post-Tensioned Concrete Structures," *ASNT Conference on NDE/NDT for Highways & Bridges: Structural Materials Technology*, 2011.
5. Bartoli, I., C. Nucera, A. Srivastava, et al., "Nonlinear ultrasonic guided waves for stress monitoring in prestressing tendons for post-tensioned concrete structures," *Proceedings of SPIE*, 729220–7292211, 2009.
6. Chen, R. H. L., K. Wissawapaisal, and E. Abramovici, "An ultrasonic method for measuring tensile forces in a seven-wire prestressing strand," *AIP Conference*, 2002.
7. Wang, Z. D., Y. Gu, and Y. S. Wang, "A review of three magnetic NDT technologies," *J. Magn. Mater.*, Vol. 324, 382–388, 2012.
8. Schoenekess, H. C., W. Ricken, W. J. Becker, et al., "Dynamic load inspection on steel tendons of steel reinforced concrete constructions by means of eddy-current sensors," *Proceedings of SPIE — The International Society for Optical Engineering*, Vol. 4337, 122–128, 2006.
9. Kim, J., J. Lee, and H. Sohn, "Automatic measurement and warning of tension force reduction in a PT tendon using eddy current sensing," *NDT & E International*, Vol. 87, 93–99, 2017.
10. Li, X., B. Zhang, C. Yuan, et al., "An electromagnetic oscillation method for stress measurement of steel strands," *Measurement*, Vol. 125, 330–335, 2018.

11. Wang, M. L., "Application of EM stress sensors in large steel cables," *Smart Struct. Syst.*, 5765, 2005.
12. Tang, D., S. Huang, W. Chen, et al., "Study of a steel strand tension sensor with difference single bypass excitation structure based on the magneto-elastic effect," *Smart Mater. Struct.*, 2008, Vol. 17, 25019.
13. Cappello, C., D. Zonta, H. A. Laasri, et al., "Calibration of elasto-magnetic sensors on in-service cable-stayed bridges for stress monitoring," *Sensors (Basel, Switzerland)*, Vol. 18, 466, 2018.
14. Duan, Y., R. Zhang, C. Dong, et al., "Development of Elasto-Magneto-Electric (EME) sensor for in-service cable force monitoring," *Int J. Struct. Stab. Dy.*, Vol. 16, 1640016, 2016.
15. Zhang, S., J. Zhou, Y. Zhou, et al., "Cable tension monitoring based on the elasto-magnetic effect and the self-induction phenomenon," *Materials*, Vol. 12, 2230, 2019.
16. Liu, L., S. Zhang, Y. Qu, et al., "Stress monitoring of prestressed steel strand based on magnetoelastic effect under weak magnetic field considering material strain," *Progress In Electromagnetics Research C*, Vol. 104, 157–170, 2020.
17. Seekircher, J. and B. Hoffmann "New magnetoelastic force sensor using amorphous alloys," *Sensors and Actuators A: Physical*, Vol. 22, 401–405, 1990.
18. Jiles, D. C., J. B. Thoenke, and M. K. Devine, "Numerical determination of hysteresis parameters for the modeling of magnetic properties using the theory of ferromagnetic hysteresis," *IEEE T. Magn.*, Vol. 28, 27–35, 1992.
19. Jiles, D. C., "Theory of the magnetomechanical effect," *Journal of Physics D: Applied Physics*, Vol. 28, 1537–1546, 1995.
20. Sablik, M. J., S. W. Rubin, L. A. Riley, et al., "A model for hysteretic magnetic properties under the application of noncoaxial stress and field," *J. Appl. Phys.*, Vol. 74, 480–488, 1993.
21. Zhang, S., J. Zhou, H. Zhang, et al., "Influence of cable tension history on the monitoring of cable tension using magnetoelastic inductance method," *Structural Health Monitoring*, 84060946, 2021.
22. Ata, N., S. Mihara, and M. Ohtsu, "Imaging of ungrouted tendon ducts in prestressed concrete by improved SIBIE," *NDT & E International*, Vol. 40, No. 3, 258–264, 2007.
23. Zapata, J., R. Vilar, and R. Ruiz, "An adaptive-network-based fuzzy inference system for classification of welding defects," *NDT & E International*, Vol. 43, No. 3, 191–199, 2010.